ACS Partner Journal

CHEMICAL & BIOMEDICAL IMAGING

Open Access

pubs.acs.org/ChemBioImaging

Article

Fluorescent Molecular Rotors Quantify an Adjuvant-Induced Softening of Plant Wax

Petr S. Sherin,* Markus Rueckel,* and Marina K. Kuimova*

Cite This: *Chem. Biomed. Imaging* 2024, 2, 453−461

Read Online

ACCESS | Metrics & More | Article Recommendations | Supporting Information

ABSTRACT: Epicuticular wax is the outmost layer of plant leaves that protects them from desiccation and penetration of harmful reagents. There is an intense industrial effort in the development of softening agents, adjuvants, that can adjust the permeability of the wax toward pesticides and, thus, play an important role in sustainable agriculture. However, mechanistic understanding of the structure and dynamic properties within the plant wax, particularly upon the application of adjuvants, is currently lacking. In this work, we demonstrate that fluorescence lifetime imaging microscopy (FLIM) combined with molecular rotors, fluorescent probes sensitive to viscosity, can directly probe the microviscosity of amorphous and crystalline phases of model plant wax layers. Moreover, this approach is able to quantify the changes in viscosity in both phases upon the addition of water and adjuvant solutions on top of the wax. We show that water permeation mostly perturbs the crystalline phase of the wax, while our chosen adjuvant, Plurafac LF431, mainly softens the amorphous phase of the wax. Our technique provides a facile and quantitative way to monitor dynamic properties within plant waxes with diffraction-limited resolution and reveals the effect of organic substances on wax structure and rigidity, crucial for designing next-generation agents to improve agricultural efficiency.

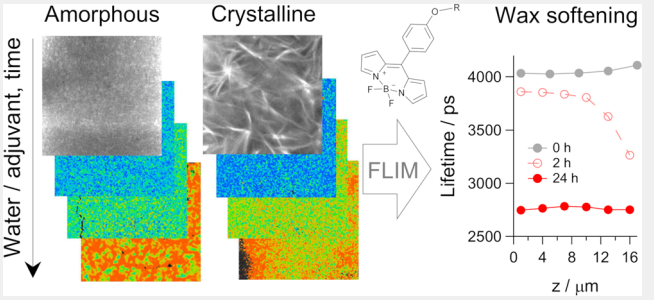

KEYWORDS: *carnauba wax, amorphous and crystalline phases, molecular rotor, BODIPY, viscosity, emulsifier, adjuvant*

INTRODUCTION

Leaves of all land plants are covered by an extracellular hydrophobic layer, plant cuticle, protecting them against desiccation and external environmental stresses.[1] Having control over the permeability through leaf cuticles is of great importance in an effort to increase the sustainability of agriculture and feeding the world's population. Currently, this control is ensured by the application of complex formulations, where adjuvants play a crucial role in increasing the permeability of the active ingredient through the leaf cuticle, which is the transport-limiting barrier for systemic pesticides. Additionally, these formulations improve wetting and adhesion of sprayed droplets on leaf surfaces. A better understanding of the structure and dynamic properties of epicuticular wax, the outer surface of the leaf cuticle, is required to develop novel adjuvants with the desired properties and effectively soften plant leaf cuticles.

Carnauba wax is an epicuticular wax extracted from the leaves of a Brazilian palm tree (*Copernicia prunifera*/*Copernicia cerifera* Martius), which is well suited as a model system to replicate plant cuticles as thin films[2] and is used for studies of the softening effects of adjuvants. This natural plant-based wax is mainly composed of long alkyl esters, diesters of cinnamic acid, and alcohols.[2,3] Though this composition is typical for leaf waxes, it can vary from species to species.[4]

A variety of methods have been applied to characterize epicuticular waxes and their softening by adjuvants, including magnetic resonance spectroscopy,[5,6] differential scanning calorimetry,[7] quartz crystal microbalance with dissipation monitoring,[8] localized thermal analysis,[9] and atomic force microscopy.[10] These studies have shown that epicuticular waxes exhibit a semicrystalline structure, where two main phases, amorphous and crystalline, are mixed. Thus, the softening effect of an adjuvant could be due to two, potentially concomitant, effects: (i) an increased presence of amorphous domains versus crystalline domains, decreasing the tortuosity and accelerating the permeation of active ingredients through the wax (shorter path length) and (ii) an increased fluidity of the amorphous phase (creating more free volume for diffusion) by the incorporation of adjuvant/water. However, despite significant interest in the effect of adjuvants on carnauba wax properties, most studies of the effect of adjuvants to date have been indirect and did not allow one to visualize the spatiotemporal profile of

Received: January 11, 2024
Revised: April 24, 2024
Accepted: April 27, 2024
Published: May 7, 2024

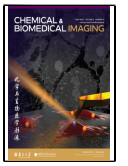

https://doi.org/10.1021/cbmi.4c00005
Chem. Biomed. Imaging 2024, 2, 453−461

adjuvant effects or the details involved in the softening mechanism.

Here we propose a new method based on fluorescence detection from environmentally sensitive fluorophores, namely molecular rotors, that could be directly incorporated into a wax layer. In molecular rotors, fluorescence intensity and lifetime increase dramatically in an environment of increased viscosity, in response to a restriction of intramolecular rotation that leads to a population of a dark, nonemissive state of the rotor.[11−13] Importantly, fluorescence lifetime could be visualized with diffraction-limited resolution using fluorescence lifetime imaging microscopy (FLIM). The lifetime (τ) response to viscosity (η) follows well-established trends[11−13] (see Figure S1 in the Supporting Information (SI)) and is insensitive to the dye concentration, therefore avoiding artifacts associated with varied uptake of a rotor within a heterogeneous object. The molecular rotor-based approach was previously successfully applied to quantify the viscosity within aerosols,[14] model lipid bilayers,[15,16] plasma membranes of live cells,[17,18] ex vivo tissues,[19,20] plant roots,[21] and mitochondrial membranes,[22,23] among others. We propose to utilize this quantitative approach to directly observe the crystalline and amorphous phases in the wax and monitor the adjuvant-induced softening in real time.

EXPERIMENTAL METHODS

Materials

The synthesis of the molecular rotors **B10**,[24] **B6++**[17] and **Thio**[25] was reported previously. The carnauba wax from Sigma-Aldrich (product no. 243213) and the emulsifier (Agnique CSO-40, purity >99.5%) and adjuvant (Plurafac LF431, purity >99.5%) from BASF were used as received. Chloroform (spectroscopic grade) was obtained from Sigma-Aldrich. To simulate agricultural conditions, tap water was used in all experiments.

Wax Staining with Fluorescent Dyes

The solid wax (10 mg) and chloroform (80 μL) were placed in a glass vial. For stock solutions, each fluorescent dye was dissolved in chloroform at a concentration of 3 mM for **B10** and **Thio** and a concentration of 0.5 mM for **B6++** and stored at −20 °C. Small aliquots of the dye stock solutions were added to the wax in chloroform in quantities of 300 ppm to the dry wax weight. These glass vials were heated up to 70 °C with a digital heater (model no. 949303, VWR International, U.S.) to achieve complete melting of the wax until it formed a homogeneous solution. Then, the hot mixtures were deposited onto preheated (75 °C) coverslips (1.0 class borosilicate glass, 22 × 50 mm, VWR International, Germany). Fast evaporation of the chloroform provided a quick and even distribution of the wax over the coverslip with a thickness variation in the range of 12−20 μm. The samples of wax on the coverslips were slowly cooled on a heating plate (MR Hei-Standard, Heidolph, Germany) at a rate of 20 °C/min for 15 min and used in further experiments.

Exposure of Wax to Aqueous Solutions

The long-term exposure of wax to aqueous solutions required the retention of the solution without evaporation. Thus, a well was formed around the wax with a volume of 200−500 μL. For this purpose, we used plastic grids from 8-well chambered microscope slides (Lab-Tek Nunc II, part no. 155411, Thermo Fisher Scientific, Germany). The plastic grid, obtained after the removal of the coverslip from the microscope slide, was placed over the melted wax before the samples were completely cooled and gently pressed to remove the wax from underneath all plastic edges. After the slow cooling of the wax samples was completed, the plastic grid was fixed on the coverslip with superglue to prevent grid displacement and water leakages during the experiments. Aliquots of 300 μL of tap water in the absence or presence of 1000 ppm emulsifier or adjuvant were added to individual wells. The whole plastic grid was covered by a coverslip to prevent water evaporation. The confocal and FLIM images were recorded at different time intervals after exposing the wax to aqueous solutions.

Multiphoton Fluorescence Imaging

Multiphoton fluorescence imaging of the wax samples stained with various dyes was performed using an inverted confocal laser-scanning microscope (Leica TCS SP5 II, Leica Microsystems, Ltd., Germany). Room-temperature imaging was carried out with a 63× (numerical aperture (NA) = 1.2) HCX PL APO CS water immersion objective lens with a correction collar (11506279, Leica Microsystems, Ltd., Germany). All fluorescent dyes were excited at 930 nm with a Ti:sapphire pulsed laser source (680−1080 nm, 80 MHz, 140 fs, Chameleon Vision II, Coherent, Inc., Germany), and the emission intensity was recorded at 490−700 nm for all dyes.

Fluorescence Lifetime Imaging Microscopy (FLIM)

FLIM images of 256 × 256 pixels were obtained using the same Leica TCS SP5 II microscope with a 63× objective coupled with a TCSPC module SPC830 (Becker & Hickl, Germany) and an internal FLIM detector PMH-100 (Becker & Hickl, Germany), synchronized to the Ti:sapphire pulsed laser.

Temperature variations were achieved with a Peltier-based heating stage for inverted microscopes (PE100-DMI) equipped with a digital controller (T96-P); both units are from Linkam Scientific Instruments (U.K.). The excitation and emission were performed with a 10× (NA = 0.3) HC PL FLUOTAR dry objective (11506505, Leica Microsystems, Ltd., Germany) with a large working distance (11 mm) to minimize the impact of the objective body (at room temperature) on the sample temperature. Samples were left to equilibrate for 15 min before each measurement.

Excitation was performed at 930 nm for all molecular rotors. For the BODIPY-based molecular rotors **B10** and **B6++**, the emission was captured at two wavelength ranges to check for possible dye aggregation: 500−580 nm (monomers) and 590−670 nm (aggregates).[15] In the case of a thiophene-based molecular rotor **Thio**, the emission was recorded at 500−700 nm. The laser power was maintained at <80 mW before entering the microscope to avoid photodamage (<0.3 μW on the sample). The acquisition time was varied in the range of 60−180 seconds per frame, depending on the emission intensity from each dye. FLIM data were recorded as a z-stack at different distances from the bottom (z = 0 μm) to the top of the wax layer (ca. 12−20 μm, depending on wax thickness) with a step size of 3−5 μm.

FLIM data were analyzed with the SPCImage v.8.3 software (Becker & Hickl, Germany) using a model of incomplete exponential decay with offset values fixed to zero. The maximum likelihood entropy (MLE) fitting algorithm was used, particularly suitable for low-intensity signals.[26] The minimal binning of pixels (bin 1, 3 × 3 pixels) was used for all data to produce a typical peak count in the decay maximum in the range of 100−200 counts per pixel (which is deemed sufficient for the MLE analysis); thresholding was adjusted from sample to sample to remove pixels of low intensity from the analysis. All decays were fitted using a monoexponential decay function for **B10** and **B6++** and a biexponential function for **Thio** with $1.0 < \chi^2 < 1.3$. A pseudocolor scale was assigned to each fluorescence lifetime, amplitude, and goodness of fit (χ^2) values (red for small values and blue for large values) to provide corresponding maps. The lifetime values and errors presented in the text are mean values and standard deviations calculated from histograms corresponding to one FLIM data frame (total amount of pixels in the range of 40 000−65 536). The reproducibility of the data was confirmed in at least two independent experiments; at least three frames were collected per condition.

RESULTS AND DISCUSSION

Choice of Molecular Rotors

The chemical structures of the molecular rotors used in this work are shown in Chart 1. We chose two BODIPY-based molecular rotors, **B10** and **B6++**, and a thiophene-based molecular rotor, **Thio**. All rotors have been characterized

https://doi.org/10.1021/cbmi.4c00005
Chem. Biomed. Imaging 2024, 2, 453−461

Chart 1. Chemical Structures of Molecular Rotors Used in This Study

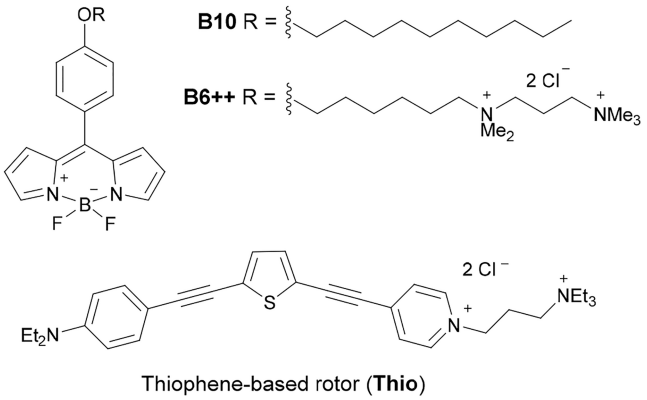

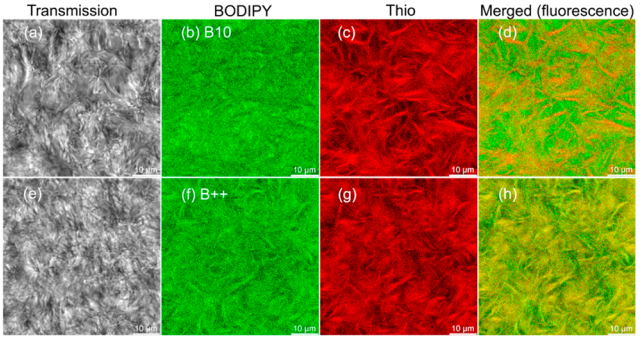

Figure 1. (a, e) Transmission and (b–d, f–h) fluorescence intensity images of carnauba wax samples co-stained with (a–d) **B10** and **Thio** and (e–h) **B6++** and **Thio** rotors. Excitation was at 930 nm, and emission detection occurred at 500–580 nm for **B10**/**B6++** and 500–700 nm for **Thio**. The scale bars are 10 μm.

previously[16,18,24,27–29] and have been used for measuring the viscosity of lipid membranes, which suggested that they might be compatible with carnauba wax due to similarities in the compositions of lipid bilayers and wax. While **B10** is a hydrophobic molecule without charge, **B6++** and **Thio** both bear positive charges, which we hypothesized might affect their partitioning within the wax.

In molecular rotors, the decay of the excited state to the ground state proceeds either via fluorescence (radiative) or intramolecular rotation with the transition into a dark state (nonradiative), which compete with each other. Since the twisting motion leading to nonradiative decay is sensitive to the viscosity of the environment, molecular rotors can be used as fluorescent sensors of local (micro)viscosity.[11–13] The response from molecular rotors can be recorded in terms of both fluorescence intensity and fluorescence lifetime.[11–13] However, the main advantage of lifetime measurements is their independence of dye uptake, which is particularly important in complex heterogeneous samples, such as plant waxes, as well as in live cells and tissues. Our previous work showed that there is a good correlation between fluorescence lifetimes of molecular rotors (intramolecular rotation) and diffusion coefficients measured by fluorescence correlation spectroscopy, FCS (translational motion)[29] as well as rotational anisotropy (rotational diffusion)[28,29] and lipid packing derived from molecular dynamic simulations.[29,30]

The viscosity dependent responses from all the molecular rotors used here were previously calibrated in well-characterized sets of solvents of known viscosity, $\tau(\eta)$, e.g., methanol/glycerol or toluene/castor oil binary mixtures;[16,18,24,27–29] see Figure S1 for **B10** and **B6++** as examples. Using the calibration curves $\tau(\eta)$, maps of lifetimes could be translated to maps of viscosity using FLIM.

Visualization of Amorphous and Crystalline Phases of Wax

Multiphoton-excited (MPE) images of the wax show significantly different staining by the neutral rotor **B10** and the positively charged molecular rotors **B6++** and **Thio** (Figure 1). While both **B6++** and **Thio** demonstrate the presence of domains with distinct needle-like structures (Figure 1c,f,g), **B10** exhibits a diffuse staining pattern (Figure 1b). However, needle-like patterns are seen in the transmission images of all samples (Figure 1a,e), indicating the existence of two different subdomains within the wax. It should be noted that MPE provides intrinsic optical sectioning (approximately 1 μm in z with a 63× objective), thus avoiding artifacts associated with variations in dye absorption and/or light scattering of the laser beam propagating within the wax.

These needle-like and fibrous structures within different plant waxes are typically assigned to the crystalline phase.[31,32] Due to the visual similarities in the patterns observed here to those reported in refs 31 and 32, we assigned the **B6++** and **Thio** staining to the crystalline phase within the wax, while we assigned the **B10** staining to the amorphous phase. The nature of the partitioning of these dyes into different phases is unclear at present, but a positive charge seems to be required for staining the crystalline phase, likely because negatively charged fatty acids are enriched therein. Thus, with available molecular rotors, we are able to discriminate between the two different phases by fluorescence microscopy for the first time.

Thio is a red-emitting molecular rotor (λ_{em}^{max} = 590 nm), as compared to the green-emitting BODIPY-based **B10** and **B6++** molecular rotors (λ_{em}^{max} = 515 nm); see Figure S2. This provides an opportunity for the simultaneous visualization of different phases in one wax sample using dual-color detection, which is illustrated in Figure 1. The lack of co-localization is seen in the images recorded within **B10** and **Thio** (Figure 1d), confirming that these dyes stain two different phases. Excellent co-localization of the images recorded within **B6++** and **Thio** (demonstrated by the dominant yellow color in Figure 1h) confirms the co-staining of a single phase by the two dyes.

Viscosity Measurements within Amorphous and Crystalline Phases of Wax

Figure 2 illustrates a typical data set obtained by FLIM, utilizing a **B6++** molecular rotor. The intensity image in Figure 2a shows the distribution of the dye across the frame. A time-resolved fluorescence decay trace is collected in each pixel of the image (red, Figure 2b). These traces could be fitted by a monoexponential function. The fitting of data in all pixels provides a map of lifetimes, represented in the pseudocolor scheme in Figure 2c, where fast decays are shown in red and long decays are shown in blue. The overall distribution of lifetimes in the image is given in a histogram (Figure 2d), which is useful for error and statistical analyses via full width at half-maximum (fwhm).

The monoexponential decay function provided a good fit for all data points in the images stained with **B6++** (Figure 2b, red). Also, despite the needle-like pattern in the intensity image (Figure 2a), a uniform distribution of lifetimes could be seen across the whole frame (Figure 2c) and at different z-positions

https://doi.org/10.1021/cbmi.4c00005
Chem. Biomed. Imaging 2024, 2, 453–461

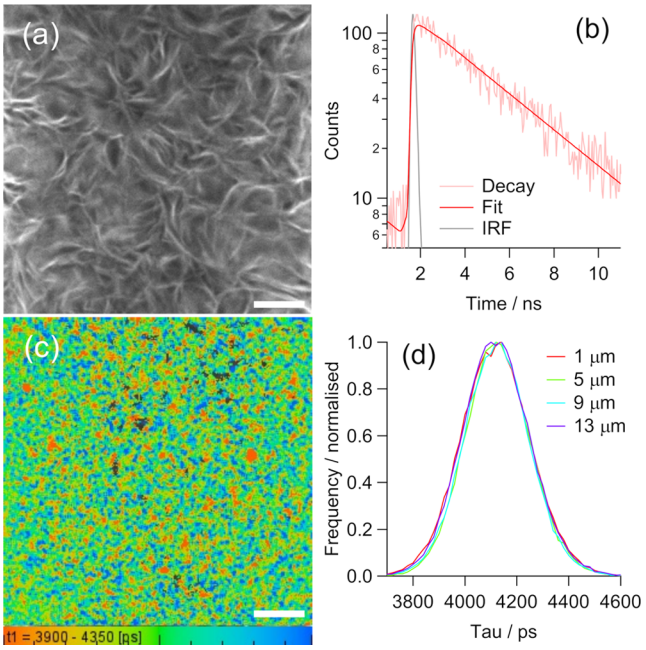

Figure 2. (a) Fluorescence intensity image of a carnauba wax sample stained with 150 ppm **B6++** after excitation at 930 nm and emission detection at 500−580 nm. (b) A typical fluorescence decay trace and the fit according to an incomplete monoexponential function. (c) FLIM image illustrating the distribution of lifetimes between 3.90 (red) and 4.35 ns (blue). (d) Distribution of **B6++** lifetimes over the whole frame at different *z*-positions through the wax layer. Image size: 61 × 61 μm; the scale bars are 10 μm.

within the wax (Figure 2d). This is consistent with a single-phase localization of the molecular rotor within the wax, i.e., even the weakly stained diffuse regions represent the rotor in the crystalline phase.

It should be noted that the wax layer itself is yellow in color, indicating its absorbance in the visible spectral region. Fluorescence intensity images and FLIM data of the wax were recorded without any fluorescent dye staining (see Figure S3 for details). Our data demonstrate that the wax exhibits some autofluorescence (Figure S3a,b) with a broad emission band with a maximum at 525 nm (Figure S3e). However, at appropriate rotor concentrations (see the SI), we see a negligible contribution of autofluorescence to the observed decays.

BODIPY-based dyes are known for their ability to form aggregates that lead to a significant shortening of lifetimes for monomeric forms.[15] To verify whether any rotor aggregates might be present within the wax, we performed FLIM experiments with wax samples stained with different concentrations of **B10** and **B6++** (75−300 ppm). Our results for lifetime distributions were independent of the dye concentration (see Figure S4a for **B10** data). Together with the monoexponential decays observed at all conditions, these data indicate the dominance of monomeric forms for the BODIPY-based molecular rotors within the wax.

Temperature variation is a convenient way to confirm that BODIPY-based molecular rotors sense their environment's viscosity rather than binding. It was previously shown that in the monomeric form, the photophysical behavior of **B10** and **B6++** is insensitive to temperature,[16] and instead, they are able to directly visualize temperature-induced changes in the viscosity of their surrounding media.[19,29] A control experiment revealed a significant decrease in **B10** lifetime within wax upon a temperature increase from 10 to 60 °C (Figure S4b). These data confirm that **B10** is functioning as a molecular rotor within the wax and is indeed sensing viscosity, as expected.

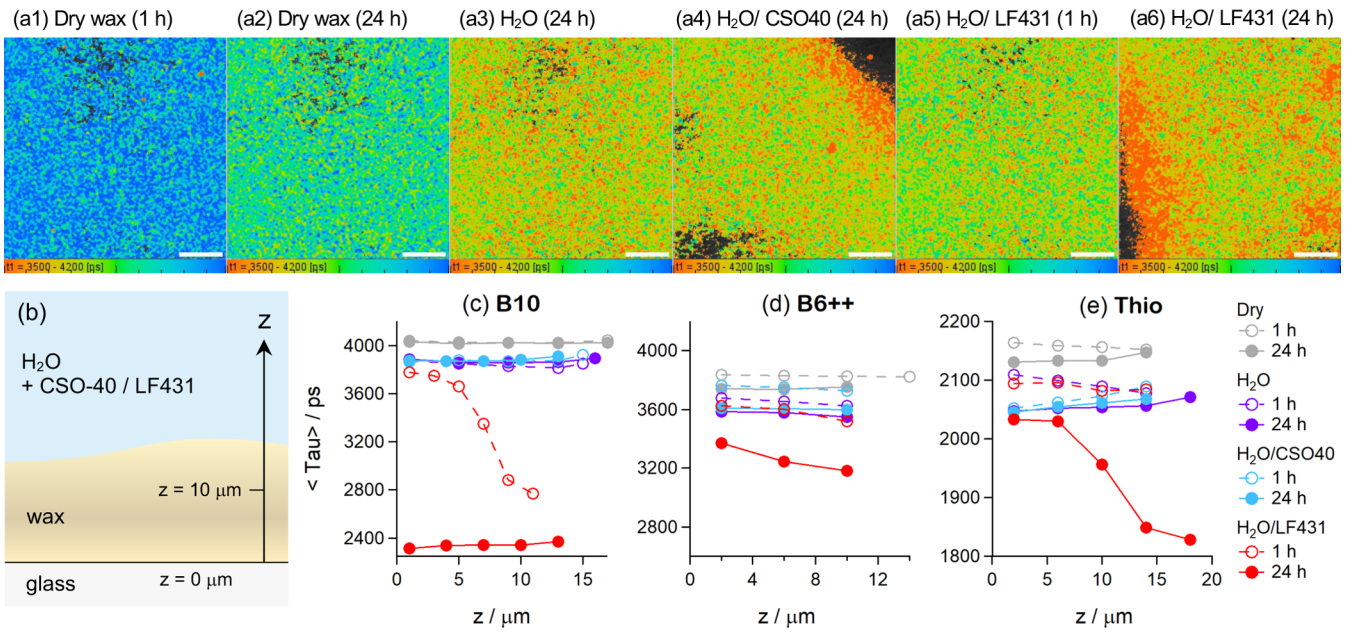

Figure 3. (a1−a6) FLIM images of carnauba wax samples stained with 150 ppm **B6++** under four different conditions: (a1, a2) untreated wax and wax stained with (a3) pure water in the absence and presence of 1000 ppm (a4) emulsifier Agnique CSO-40 or (a5, a6) adjuvant Plurafac LF431 (a1, a5) 1 h and (a2−a4, a6) 24 h after the start of the experiment. Images were recorded with excitation at 930 nm and emission detection at 500−580 nm for **B10**/**B6++** and 500−700 nm for **Thio**. The scale bar for all images is 40 μm; the full sets of images can be found in the SI, Figures S6−S8. (b) Schematic representation of exposing the wax to aqueous solutions containing the emulsifier or the adjuvant; all images are given for the lowest positions within the wax, $z \approx 1-2$ μm. (c−e) *z*-profiles of recorded lifetimes for (c) **B10**, (d) **B6++**, and (e) **Thio** within waxes stained under various conditions, as indicated in the figure legend on the right.

https://doi.org/10.1021/cbmi.4c00005
Chem. Biomed. Imaging 2024, 2, 453−461

Using the calibration curve for **B10** (Figure S1),[16] we translated the lifetimes to values of viscosities within the amorphous phase of wax: 905 ± 90 cP at 10 °C, 820 ± 80 cP at 25 °C, 715 ± 70 cP at 40 °C, and 620 ± 50 cP at 60 °C. It should be noted that molecular rotors within the crystalline phase report distinctly different viscosity values: while **B6++** reports 435 cP at 19 °C, the **Thio** lifetime values seen within the wax exceed the values previously reported for this dye at viscosities of 1−975 cP.[18,27] The high viscosity values of >1000 cP seen with **Thio** are consistent with the high packing expected in the crystalline phase of the wax; however, the low viscosity values seen with **B6++** are unexpected. While the lifetime of these positively charged dyes remains sensitive to temperature (see below) and the presence of adjuvants (see Figure 3), we exercise caution when interpreting viscosity values resulting from **B6++** and **Thio**, as their lifetimes may be determined by fixed geometries with insufficient freedom for rotation due to the tight packaging of the crystalline phase.

It should be noted that the lifetimes measured with all dyes did not change over long periods of wax storage of more than one year (wax samples were stored under dry and dark conditions). This indicates carnauba wax as a chemically inert environment for the molecular rotors used and high reproducibility of the suggested approach.

Wax Softening upon Penetration of Water and Adjuvant

Molecular rotors provide a unique opportunity to visualize and quantify the changes to wax packing for both amorphous and crystalline phases, which is a sought-after measurement, particularly during dynamic perturbations, e.g., upon contact with agriculturally relevant formulations. We set out to test the effect of pure water and two aqueous solutions of commonly used agrochemicals on the structure of wax phases: a nonionic emulsifier typically used to stabilize formulations, Agnique CSO-40, and a softening adjuvant, Plurafac LF431.

For this purpose, we recorded four parallel data sets under the following conditions: (i) dry wax, (ii) waxes exposed to water, and waxes exposed to aqueous solutions of 1000 ppm (iii) emulsifier (Agnique CSO-40) and (iv) adjuvant (Plurafac LF431). Agnique CSO-40 is assumed to have no impact on the wax structure and function, while Plurafac LF431 is considered to soften the wax. All wax samples were stained with aqueous solutions simultaneously in our custom-designed chamber (see Figure S5); each wax sample was stained with only one molecular rotor at a time. Two independent sets of measurements were carried out for each dye within the wax.

FLIM data sets were obtained at different time intervals after exposing the wax to these aqueous solutions. Typical FLIM images are given in Figure 3a1−a6; the expanded data sets and fluorescence intensity and FLIM images for each molecular rotor are given in Figures S6−S8. Data were recorded at different z-positions within the wax to assess the spatiotemporal effect of solutions placed on top of the wax layer. See Figure 3b for a schematic of how z was defined. Complete z-profiles of changes to the rotor lifetimes upon the penetration of water and chemicals as a function of z are given in Figure 3c−e.

Our results clearly show differences between the impacts of water and organic substances on both the amorphous and crystalline phases of carnauba wax. While the lifetime of **B10**, visualizing the amorphous phase, decreases only slightly upon the penetration of water (purple data set, Figure 3c), the lifetime shows a stark decrease upon the treatment with the adjuvant. Its propagation inside the wax could be clearly visualized by the corresponding z-profiles (open red circles, Figures 3c and S9). While the dynamics of the lifetime reduction depends on the thickness of the wax layer (e.g., compare the data from two repeats, Figures 3 and S9), the trend of significant softening of the amorphous phase by the adjuvant is clear. The complete saturation of the wax with Plurafac LF431 can be seen at later times in the experiment (shaded red circles, Figure 3c). The effect of the emulsifier Agnique CSO-40 on the **B10** lifetime is very similar to the effect of pure water (light blue dots, Figure 3c), which indicates its minor impact on the amorphous phase structure, packing and, potentially, permeability.

The molecular rotors within the crystalline phase, namely **B6++** and **Thio** (Figure 3d,e), also exhibit small changes in lifetimes upon water penetration (purple) as compared to the dry wax (gray). The presence of the emulsifier in the aqueous solution has a minor impact on the lifetimes of **B6++** and **Thio** within wax (blue circles) as compared to water (purple circles). In the case of the adjuvant, at the early stages of the experiments, the presence of Plurafac LF431 does not appear to play a role; however, crystalline phase softening is seen at later times. We saw slight variation in the timing of this softening from sample to sample (see Figure S9 for z-profiles obtained in a repeat set of experiments), possibly due to different wax layer thicknesses. It is worth noting that the fast softening effect was highly reproducible for the amorphous phase, monitored with **B10**. These differences in timing could be due to a significantly higher packing/viscosity of the crystalline phase.

Another interesting feature measured by **B6++** and **Thio** is the decrease of lifetimes in the dry wax within 1 day after the sample preparation (open and shaded gray circles), which is reproducible for two independent measurements (see Figure S9). This effect was not observed in the case of **B10**, which stained the amorphous phase (Figures 3c and S9). We speculate that this decrease is due to the penetration of water from the atmosphere inside the wax, which has a softening effect on the crystalline phase only. As the uppermost layer of the leaf cuticle is constantly exposed to humidity in the atmosphere, we can consider these values as a more realistic representation of the apical packing of the crystalline phase in the wax.

It is important to note that no visual changes in the patterns of staining of the crystalline phase were visualized by **B6++** and **Thio**, even after prolonged exposure of the wax layer to the adjuvant (Figure S10). We continue to see the needle-like structure of the crystalline phase of the wax even after the penetration of Plurafac LF431. This indicates that rather than dissolving the crystalline domains, the adjuvant is softening the amorphous phase instead, with some contribution to softening seen from pure water itself.

It should be noted that the wax layers used in this work are of higher thickness (12−20 μm) compared to those occurring naturally (<2 μm).[1] As a result, the penetration of water and organic substances in the model layers studied here may lead to morphological changes in the wax structure, which are not possible in live plant leaves. We observed the formation of cracks of various sizes in our experiments (see Figure S11 for examples), which we do not believe to be biologically relevant. Another common nonbiologically relevant side-effect seen in our experiments is the curving of the wax layer in the presence of the adjuvant, with the detachment of the wax from the coverslip seen in limiting cases (Figure S11, right column). The buckling of wax layers is consistent with the increase of wax volume upon adjuvant penetration, as was previously reported.[5,6] The

https://doi.org/10.1021/cbmi.4c00005
Chem. Biomed. Imaging 2024, 2, 453−461

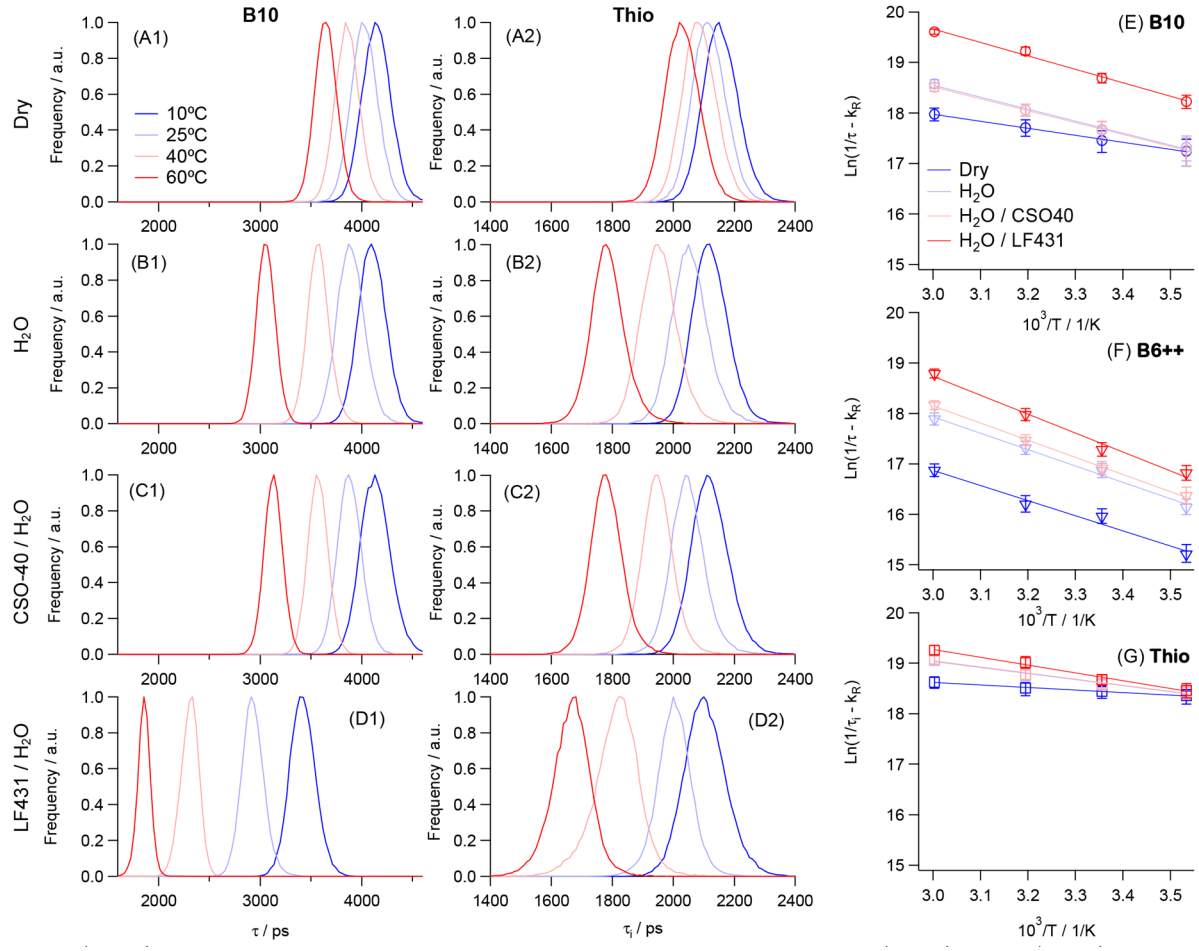

Figure 4. (A1−D2) Lifetime histograms extracted from FLIM images of carnauba wax samples stained with (A1−D1) **B10** and (A2−D2) **Thio**, recorded at different temperatures from 10 (blue) to 60 °C (red). All samples were exposed for 24 h to the following conditions: (A1, A2) dry wax and waxes exposed to (B1, B2) H_2O; (C1, C2) H_2O/CSO-40, 1000 ppm; and (D1, D2) H_2O/LF431, 1000 ppm. (E−G) $\ln(1/\tau - k_R)$ versus $1/T$ plots for (E) **B10**, (F) **B6++**, and (G) **Thio**. Solid lines: best linear fits according to eq 3.

preparation of thinner layers of wax should significantly reduce these morphological changes.

As additional controls, we measured the lifetimes of molecular rotors in the presence of various concentrations of the adjuvant to exclude that the observed decrease in lifetimes could be due to fluorescence quenching of the rotors by the adjuvant. The lifetimes of **B10** and **B6++** in different binary mixtures of dimethyl sulfoxide (DMSO) and neat adjuvant (see Figure S12) increased at high concentrations of adjuvant. This increase could be assigned to a higher viscosity of the neat adjuvant as compared to DMSO. Importantly, these control experiments rule out quenching as the source of the softening seen upon water/adjuvant penetration in our experiments.

Temperature Variation as a Tool to Study Wax Fluidity

We next sought to characterize changes in the carnauba wax structure upon water and emulsifier/adjuvant penetration upon varying the sample temperature. It is expected that a viscous fluid, such as wax, will considerably change its viscosity upon heating and cooling. Fluorescence lifetimes of BODIPY-based molecular rotors were previously shown to be temperature-independent;[16] however, **Thio** has some degree of temperature sensitivity.[27] Therefore, **B10** and **B6++** should be able to visualize the temperature-induced changes in the viscosity of wax, while **Thio** may have some viscosity independent contribution to the observed changes in the signal.

FLIM data at different temperatures were obtained with wax layers at the same conditions tested before, at a single z-position, after 24 h of staining (see Figure S9 for the full z-profiles). The temperature range of 10−60 °C was chosen due to wax melting at higher temperatures and it being readily available within the existing FLIM microscopy setup. The changes in the lifetime distributions upon temperature variation are shown in Figure 4 for **B10** and **Thio** and in Figure S13 for **B6++**. The changes in the observed lifetimes as a function of temperature for all three molecular rotors are given in Figure S14.

The ingress of water increases the sensitivity of the rotor lifetimes within wax to temperature for both the amorphous and crystalline phases (Figures 4B1,B2 and S13). This could be clearly seen by an increase of gradients of $\ln(1/\tau - k_R)$ versus $1/T$ graphs (Figure 4E−G), with slopes yielding apparent activation energy values for each condition. The presence of the emulsifier in the aqueous solution has a negligible effect on the temperature sensitivity of both phases as compared to pure water (Figure 4C1,C2,E−G). In contrast, the presence of the adjuvant has a large impact on the amorphous phase, visualized by **B10** (Figure 4D1), and a modest effect on the crystalline phase stained with **B6++** and **Thio** (Figures S13 and 4D2,

https://doi.org/10.1021/cbmi.4c00005
Chem. Biomed. Imaging 2024, 2, 453−461

respectively). These results are in good agreement with the *z*-profiles presented in Figures 3 and S9.

The analysis of temperature sensitivity was done within a simple model describing the decay of the molecular rotor excited states by two competing processes: a radiative decay via fluorescence and a nonradiative decay (viscosity and temperature-dependent), with the corresponding rate constants k_R and k_V:

$$\tau = 1/(k_R + k_V) \quad (1)$$

$$k_V = A_V \exp\left(-\frac{E_{AV}}{RT}\right) \quad (2)$$

where τ is the fluorescence lifetime, A_V is the pre-exponential factor, E_{AV} is the activation energy, R is the gas constant, and T is the temperature in kelvin.

We note that viscosity (particularly that of viscous fluids) strongly depends on temperature. Therefore, the Arrhenius term k_V (eq 2) incorporates both the intrinsic temperature sensitivity of the nonradiative decay (expected to be low)[16,27] and the temperature-dependent environmental viscosity. Separate treatment of both contributions was attempted previously for BODIPY-based rotors[16] but is outside the scope of the current study.

k_R is nearly temperature-independent for **B10** in a range of methanol/glycerol solutions (see Figure S15 and the related section in the SI for details). Thus, if k_R is temperature-independent for all rotors, this model predicts the following linear relationship:

$$\ln(1/\tau - k_R) = \ln(A_V) - \frac{E_{AV}}{RT} \quad (3)$$

Figure 4E−G shows the fitted plots of $\ln(1/\tau - k_R)$ versus $1/T$ for all three molecular rotors within waxes. Linear fits are given as solid lines for the k_R values fixed for each rotor (see the SI for details); the values for E_{AV} obtained from these fits are listed in Table 1. Good linearities were observed for all molecular rotors (see Figure S16 for individually expanded *y*-axis scales for each molecular rotor), which gives us confidence in the suitability of this model for all dyes used.

Table 1. Activation Energies (E_{AV}) Extracted from Linear Fits in Figure 4E−G, According to Eq 3

	E_{AV} (kJ mol^{-1})		
wax staining	**B10**	**B6++**	**Thio**
dry	11.5	24.9	4.1
H_2O	19.7	27.1	9.9
H_2O/CSO-40	19.5	28.2	10.0
H_2O/LF431	22.1	31.3	12.8

Given that the photophysics of BODIPY-based molecular rotors was previously shown to be mostly temperature-independent[16] and that **Thio** rotors showed slight temperature sensitivity,[27] we expected that the variations in the E_{AV} values would mostly reflect the changes in the viscosity of the amorphous (**B10** data) and crystalline phases (**B6++** and **Thio** data) of wax upon changing the temperature in the vicinity of these molecular rotors. In other words, we expected higher E_{AV} values from higher-viscosity environments (see Figure S17 for the behavior of **B10** in methanol/glycerol mixtures).

However, in the case of wax measurements with **B10** and **Thio**, the higher E_{AV} values seen in the water and adjuvant-infused wax correspond to lower rotor lifetimes (lower viscosity). One possible interpretation of this data is that in some cases, the rotors experience specific steric interactions (i.e., binding). The temperature variations are expected to have a minor effect on binding.

The **Thio** rotor demonstrates the lowest E_{AV} values among all the molecular rotors used (Table 1). We note that its lifetimes recorded at all conditions are outside the upper bounds of the viscosity calibration range (1.5 ns at 975 cP).[18,27] **Thio** within wax exhibits a very bright fluorescence signal, which is in stark contrast to our previous observations of low emission signals from **Thio** in methanol/glycerol and toluene/castor oil mixtures from lipid vesicles[18,27] and plasma membranes of live cells.[19] The bright intensity, unexpected long lifetimes, and weak temperature sensitivity indicate that **Thio** is most likely tightly bound to wax components.

B6++ shows the highest E_{AV} values at all conditions studied (Table 1), and the lifetimes can be converted to viscosities, giving values of ∼290−435 cP (Table S3). However, we note that typically, we expect tighter packing and higher viscosities from the crystalline phase of the wax compared to the amorphous phase. Thus, we cannot exclude a quenching of **B6++** by the wax components, which would lead to an underestimation of viscosity values.

Even though the lifetimes of **B6++** and **Thio** do not appear to quantitatively correlate to the tight packing/high viscosity expected within the crystalline phase of carnauba wax, **B6++** and **Thio** sense the penetration of adjuvants within the wax by showing significant reduction of their lifetimes. Therefore, they could be used for quantitative kinetic monitoring of this process.

All our data (Figures 3, 4, S4, and S9) indicate that **B10** operates as a true molecular rotor within the wax, with activation energy values expected in viscous solvents, such as glycerol,[15,16] castor oil,[16] and lipid bilayers.[15] Therefore, the lifetimes shown in Figure 3 could be converted to viscosities (at 19 °C) using the calibration curve reported in (Figure S1):[16] 815 ± 80 cP for the untreated/dry wax, which reduces to 700 ± 50 and 205 ± 25 cP with the permeation of water and Plurafac LF431, respectively. These values, which are typical of hydrocarbon-rich domains of lipid bilayers,[15] combined with the E_{AV} values typical of lipid bilayers[15] give us confidence that these viscosities truly reflect the mobility and diffusion rates within wax. The significant reduction in the viscosity of the amorphous phase of the wax points to Plurafac LF431 as the softening agent, which could facilitate the permeation of active ingredients inside the leaf.

CONCLUSIONS

Our work demonstrates the applicability of FLIM with viscosity sensitive molecular rotors for structural and dynamic studies of plant leaf waxes. Two phases known to coexist in carnauba wax samples, namely the amorphous and crystalline phases, were visualized by changing peripheral substituents of the molecular rotors, providing us with the means to study the packing and organization of both phases separately. Our results showed that the viscosity could be quantitatively measured for the amorphous phase visualized with the molecular rotor **B10**. The viscosity values provided by the molecular rotors that stained the crystalline phase of carnauba wax, **B6++** and **Thio**, differed greatly, indicating more complex interactions in this tightly packed microenvironment with the dyes used. However, in both phases and for all rotors studied, FLIM could be used to follow changes within the wax structure upon changes in temperature and the addition of agrochemicals.

https://doi.org/10.1021/cbmi.4c00005
Chem. Biomed. Imaging 2024, 2, 453−461

Our data showed that the viscosity of the amorphous phase is weakly affected by water penetration; however, its structure is severely impacted by the dissolution of the adjuvant, which makes it significantly more liquid. The control experiment, upon the addition of an emulsifier commonly present in agrochemical formulations, illustrated that only wax softeners are able to affect the packing of the amorphous phase of the wax. The lifetimes of the molecular rotors within the crystalline phase exhibited a marked sensitivity to water penetration and were insensitive to emulsifier presence. However, the adjuvant worked to slowly soften (but not dissolve) the crystalline phase of the wax. Overall, the crystalline phase of the wax was less affected by additives (water/emulsifier/adjuvant). This observation allows us to state that the softening of the wax upon the action of Plurafac LF431, particularly at short times after application, is mostly due to the effect on the amorphous phase of the wax rather than a dissolution or softening of the crystalline domains.

Our findings open the opportunity for systematic and quantitative studies of plant waxes and their mixtures with various natural compounds[2] by means of optical microscopy. The application of functional fluorescent probes such as molecular rotors holds great promise in providing quantitative characterization as well as visualization of the impact of different chemical substances on the dynamic properties of these complex natural materials.

■ ASSOCIATED CONTENT

Supporting Information

The Supporting Information is available free of charge at https://pubs.acs.org/doi/10.1021/cbmi.4c00005.

Intensity, FLIM, and transmission images of the wax autofluorescence and the wax samples stained with **B10**, **B6++**, and **Thio** exposed to water and emulsifier/adjuvant; and the analysis of temperature effects (PDF)

■ AUTHOR INFORMATION

Corresponding Authors

Petr S. Sherin − *MSRH, Department of Chemistry, Imperial College London, London W12 0BZ, U.K.;* orcid.org/0000-0002-9169-4655; Email: p.sherin@imperial.ac.uk

Markus Rueckel − *BASF SE, Ludwigshafen am Rhein 67056, Germany*; Email: markus.rueckel@basf.com

Marina K. Kuimova − *MSRH, Department of Chemistry, Imperial College London, London W12 0BZ, U.K.;* orcid.org/0000-0003-2383-6014; Email: m.kuimova@imperial.ac.uk

Complete contact information is available at: https://pubs.acs.org/10.1021/cbmi.4c00005

Author Contributions

P.S.S.: data acquisition, data analysis, and writing of the first draft. M.R.: conceptualization and financial acquisition. M.K.K.: equipment, resources, and supervision. The manuscript was co-edited and co-written by all authors.

Notes

The authors declare no competing financial interest.

■ ACKNOWLEDGMENTS

We thank our BASF colleagues from the Industrial Formulators for their support. M.K.K. is grateful to the EPSRC for a Career Acceleration Fellowship (EP/I003983/1).

■ REFERENCES

(1) Yeats, T. H.; Rose, J. K. C. The Formation and Function of Plant Cuticles. *Plant Physiol.* **2013**, *163*, 5.

(2) Susmita Devi, L.; Kalita, S.; Mukherjee, A.; Kumar, S. Carnauba Wax-Based Composite Films and Coatings: Recent Advancement in Prolonging Postharvest Shelf-Life of Fruits and Vegetables. *Trends Food Sci. Technol.* **2022**, *129*, 296.

(3) Krendlinger, E.; Wolfmeier, U.; Schmidt, H.; Heinrichs, F.-L.; Michalczyk, G.; Payer, W.; Dietsche, W.; Boehlke, K.; Hohner, G.; Wildgruber, J. Waxes. In *Ullmann's Encyclopedia of Industrial Chemistry*; Wiley, 2015. DOI: 10.1002/14356007.a28_103.pub2.

(4) Jetter, R.; Kunst, L.; Samuels, A. L. Composition of Plant Cuticular Waxes. *Annu. Plant Rev.*. **2006**, *23*, 145.

(5) Schreiber, L.; Riederer, M.; Schorn, K. Mobilities of Organic Compounds in Reconstituted Cuticular Wax of Barley Leaves: Effects of Monodisperse Alcohol Ethoxylates on Diffusion of Pentachlorophenol and Tetracosanoic Acid. *Pest. Sci.* **1996**, *48*, 117.

(6) Schreiber, L.; Schorn, K.; Heimburg, T. ^{2}H NMR Study of Cuticular Wax Isolated from Hordeum Vulgare L. Leaves: Identification of Amorphous and Crystalline Wax Phases. *Eur. Biophys. J.* **1997**, *26*, 371.

(7) Coret, J.; Chamel, A. Effect of Some Ethoxylated Alkylphenols and Ethoxylated Alcohols on the Transfer of [14C] Chlorotoluron Across Isolated Plant Cuticles. *Weed Res.* **1994**, *34*, 445.

(8) Fagerström, A.; Kocherbitov, V.; Westbye, P.; Bergström, K.; Arnebrant, T.; Engblom, J. Surfactant Softening of Plant Leaf Cuticle Model Wax − A Differential Scanning Calorimetry (DSC) and Quartz Crystal Microbalance with Dissipation (QCM-D) Study. *J. Colloid Interface Sci.* **2014**, *426*, 22.

(9) Perkins, M. C.; Roberts, C. J.; Briggs, D.; Davies, M. C.; Friedmann, A.; Hart, C.; Bell, G. Macro and Microthermal Analysis of Plant Wax/Surfactant Interactions: Plasticizing Effects of Two Alcohol Ethoxylated Surfactants on an Isolated Cuticular Wax and Leaf Model. *Appl. Surf. Sci.* **2005**, *243*, 158.

(10) Grant, C.; Twigg, P.; Bell, G.; Lu, J. R. AFM Relative Stiffness Measurement of the Plasticising Effect of a Non-Ionic Surfactant on Plant Leaf Wax. *J. Colloid Interface Sci.* **2008**, *321*, 360.

(11) Kuimova, M. K. Mapping viscosity in cells using molecular rotors. *Phys. Chem. Chem. Phys.* **2012**, *14*, 12671.

(12) Paez-Perez, M.; Kuimova, M. K. Molecular Rotors: Fluorescent Sensors for Microviscosity and Conformation of Biomolecules. *Angew. Chem., Int. Ed.* **2024**, *63*, No. e202311233.

(13) Haidekker, M. A.; Theodorakis, E. A. Environment-sensitive behavior of fluorescent molecular rotors. *J. Biol. Eng.* **2010**, *4*, 11.

(14) Hosny, N. A.; Fitzgerald, C.; Vyšniauskas, A.; Athanasiadis, A.; Berkemeier, T.; Uygur, N.; Pöschl, U.; Shiraiwa, M.; Kalberer, M.; Pope, F. D.; Kuimova, M. K. Direct Imaging of Changes in Aerosol Particle Viscosity upon Hydration and Chemical Aging. *Chem. Sci.* **2016**, *7*, 1357.

(15) Wu, Y.; Štefl, M.; Olzyńska, A.; Hof, M.; Yahioglu, G.; Yip, Ph.; Casey, D. R.; Ces, O.; Humpolıckova, J.; Kuimova, M. K. Molecular Rheometry: Direct Determination of Viscosity in L_o and L_d lipid Phases via Fluorescence Lifetime Imaging. *Phys. Chem. Chem. Phys.* **2013**, *15*, 14986.

(16) Vyšniauskas, A.; López-Duarte, I.; Duchemin, N.; Vu, T. T.; Wu, Y.; Budynina, E. M.; Volkova, Y. A.; Peña Cabrera, E.; Ramirez-Ornelas, D. E.; Kuimova, M. K. Exploring Viscosity, Polarity and Temperature Sensitivity of BODIPY-based Molecular Rotors. *Phys. Chem. Chem. Phys.* **2017**, *19*, 25252.

(17) López-Duarte, I.; Vu, T. T.; Izquierdo, M. A.; Bull, J. A.; Kuimova, M. K. A Molecular Rotor for Measuring Viscosity in Plasma Membranes of Live Cells. *Chem. Commun.* **2014**, *50*, 5282.

(18) Dent, M. R.; López-Duarte, I.; Dickson, C. J.; Chairatana, P.; Anderson, H. L.; Gould, I. R.; Wylie, D.; Vyšniauskas, A.; Brooks, N. J.; Kuimova, M. K. Imaging Plasma Membrane Phase Behaviour in Live Cells Using a Thiophene-Based Molecular Rotor. *Chem. Commun.* **2016**, *52*, 13269.
(19) Sherin, P. S.; López-Duarte, I.; Dent, M. R.; Kubankova, M.; Vyšniauskas, A.; Bull, J. A.; Reshetnikova, E. S.; Klymchenko, A. S.; Tsentalovich, Yu.P.; Kuimova, M. K. Visualising the Membrane Viscosity of Porcine Eye Lens Cells Using Molecular Rotors. *Chem. Sci.* **2017**, *8*, 3523.
(20) Sherin, P. S.; Vyšniauskas, A.; López-Duarte, I.; Ogilby, P. R.; Kuimova, M. K. Visualising UV-A Light-Induced Damage to Plasma Membranes of Eye Lens. *J. Photochem. Photobiol. B: Biol.* **2021**, *225*, No. 112346.
(21) Michels, L.; Gorelova, V.; Harnvanichvech, Y.; Borst, J. W.; Albada, B.; Weijers, D.; Sprakel, J. Complete Microviscosity Maps of Living Plant Cells and Tissues with a Toolbox of Targeting Mechanoprobes. *Proc. Natl. Acad. Sci. U.S.A.* **2020**, *117*, 18110.
(22) Steinmark, I. E.; James, A. L.; Chung, P.-H.; Morton, P. E.; Parsons, M.; Dreiss, C. A.; Lorenz, C. D.; Yahioglu, G.; Suhling, K. (2019) Targeted Fluorescence Lifetime Probes Reveal Responsive Organelle Viscosity and Membrane Fluidity. *PLoS One* **2019**, *14*, No. e0211165.
(23) Singh, G.; George, G.; Raja, S. O.; Kandaswamy, P.; Kumar, M.; Thutupalli, S.; Laxman, S.; Gulyani, A. A Molecular Rotor FLIM Probe Reveals Dynamic Coupling Between Mitochondrial Inner Membrane Fluidity and Cellular Respiration. *Proc. Natl. Acad. Sci. U.S.A.* **2023**, *120*, No. e2213241120.
(24) Kuimova, M. K.; Yahioglu, G.; Levitt, J. A.; Suhling, K. Molecular Rotor Measures Viscosity of Live Cells via Fluorescence Lifetime Imaging. *J. Am. Chem. Soc.* **2008**, *130*, 6672.
(25) López-Duarte, I.; Chairatana, P.; Wu, Y.; Pérez-Moreno, J.; Bennett, P. M.; Reeve, J. E.; Boczarow, I.; Kaluza, W.; Hosny, N. A.; Stranks, S. D.; Nicholas, R. J.; Clays, K.; Kuimova, M. K.; Anderson, H. L. Thiophene-Based Dyes for Probing Membranes. *Org. Biomol. Chem.* **2015**, *13*, 3792.
(26) Becker, W. In *The bh TCSPC Handbook*, 8th ed.; Becker & Hickl GmbH, 2019; p 783.
(27) Páez-Pérez, M.; López-Duarte, I.; Vyšniauskas, A.; Brooks, N. J.; Kuimova, M. K. Imaging Non-Classical Mechanical Responses of Lipid Membranes Using Molecular Rotors. *Chem. Sci.* **2021**, *12*, 2604.
(28) Levitt, J. A.; Kuimova, M. K.; Yahioglu, G.; Chung, P.-H.; Suhling, K.; Phillips, D. Membrane-Bound Molecular Rotors Measure Viscosity in Live Cells via Fluorescence Lifetime Imaging. *J. Phys. Chem. C* **2009**, *113*, 11634.
(29) Dent, M. R.; López-Duarte, I.; Dickson, C. J.; Geoghegan, N. D.; Cooper, J. M.; Gould, I. R.; Krams, R.; Bull, J. A.; Brooks, N. J.; Kuimova, M. K. Imaging phase separation in model lipid membranes through the use of BODIPY based molecular rotors. *Phys. Chem. Chem. Phys.* **2015**, *17*, 18393.
(30) Paez-Perez, M.; Vyšniauskas, A.; López-Duarte, I.; Lafarge, E. J.; López-Ríos De Castro, R.; Marques, C. M.; Schroder, A. P.; Muller, P.; Lorenz, C. D.; Brooks, N. J.; Kuimova, M. K. Directly Imaging Emergence of Phase Separation in Peroxidized Lipid Membranes. *Commun. Chem.* **2023**, *6*, 15.
(31) Blake, A. I.; Co, E. D.; Marangoni, A. G. Structure and Physical Properties of Plant Wax Crystal Networks and Their Relationship to Oil Binding Capacity. *J. Am. Oil. Chem. Soc.* **2014**, *91*, 885.
(32) Wang, H.; Boyer, S. A. E.; Bellet, M.; Dalle, F. Effects of Wax Components and the Cooling Rate on Crystal Morphology and Mechanical Properties of Wax−Oil Mixtures. *Cryst. Growth Des.* **2023**, *23*, 1422.

https://doi.org/10.1021/cbmi.4c00005
Chem. Biomed. Imaging 2024, 2, 453−461